AIAA 2001-4319
Free-Flight Range Tests and Numerical Computations of a Power-Law Elliptic Cross-Section Projectile

Gregg Abate
Air Force Research Laboratory
Eglin AFB, FL

John J. Bertin, James R. Forsythe, and Paul H. Schuricht
United States Air Force Academy
U. S. Air Force Academy, CO 80840

AIAA Atmospheric Flight Mechanics
Conference & Exhibit
August 6-9, 2001/Montréal, Canada

Free-Flight Range Tests and Numerical Computations of a Power-Law Elliptic Cross-Section Projectile

Gregg L. Abate[*]
Air Force Research Laboratory Munitions Directorate
Eglin AFB, FL 32542

and

John J. Bertin[†], James R. Forsythe[‡], and Paul H. Schuricht[§]
United States Air Force Academy
U. S. Air Force Academy, CO 80840

Abstract

This paper presents computational and experimental aerodynamic data of a power-law elliptic cross-section projectile at Mach numbers ranging from 3.0 to 5.0. The experimental data consisted of nine free-flight projectiles launched within an instrumented facility. The computational work was carried out via the Cobalt$_{60}$ code at the flight conditions of the experimental facility. The results indicate good agreement between the experimental and computational data determined in this effort as well as with engineering level predictions. The free-flight data was limited to small angles of attack so high fidelity determination of the aerodynamic stability coefficients and derivatives was not possible. Discrepancies were seen in the center of pressure data between the experimental and the computational data and require further investigation.

List of Symbols

A = cross section area of the model and reference area ($A = \pi * d_{maj} * d_{min}$)

cg = center of gravity

C_l = roll moment coefficient ($C_l \equiv \dfrac{l}{\bar{q}Ad_{ref}}$)

C_m = pitch moment coefficient ($C_m \equiv \dfrac{m}{\bar{q}Ad_{ref}}$)

$C_{m\alpha}$ = pitching moment coefficient derivative ($\dfrac{\partial Cm}{\partial \alpha}$)

C_{mq} = pitch damping moment coefficient derivative ($\dfrac{\partial Cm}{\partial q}$)

C_n = yaw moment coefficient ($C_n \equiv \dfrac{n}{\bar{q}Ad_{ref}}$)

$C_{n\beta}$ = yaw moment coefficient derivative ($\dfrac{\partial Cn}{\partial \beta}$)

C_{nr} = yaw damping moment coefficient derivative ($\dfrac{\partial Cn}{\partial r}$)

C_X = axial force coefficient ($C_X \equiv \dfrac{X}{\bar{q}A}$)

C_{Xo} = zero yaw axial force coefficient

C_Y = yaw force coefficient ($C_Y \equiv \dfrac{Y}{\bar{q}A}$)

$C_{Y\beta}$ = normal force coefficient derivative in the yaw plane ($\dfrac{\partial C_Y}{\partial \beta}$)

C_Z = normal force coefficient ($C_Z \equiv \dfrac{Z}{\bar{q}A}$)

$C_{Z\alpha}$ = normal force coefficient derivative in the pitch plane ($\dfrac{\partial C_Z}{\partial \alpha}$)

d_{maj} = major diameter of the model

d_{min} = minor diameter of the model

d_{ref} = reference diameter of the model

e = elliptic cross-section eccentricity

I_x, I_y = moment of inertia about the x and y axis

k = model surface constant

l = model length

l,m,n = roll, pitch, and yaw moment about projectile cg

$p.q.r$ = roll rate, pitch rate, and yaw rate about projectile cg

$\bar{q}$ = dynamic pressure

r = radius of model surface

---

[*] Aerospace Engineer, Senior Member AIAA
[†] Professor of Aeronautics, Fellow of AIAA
[‡] Assistant Professor, Member AIAA
[§] Post-Doctoral Research Fellow

X_{CG}	=	location of center of gravity measured from nose
$X_{c.p.}$	=	location of center of pressure measured from nose
x,y,z	=	downrange, side, and vertical position coordinates
X,Y,Z	=	axial, yaw, and normal body forces
z	=	vertical position coordinate
α	=	pitch angle
$\overline{\alpha}$	=	total angle of attack
β	=	yaw angle
θ	=	angular coordinate of model surface

Introduction

Background

The use of highly maneuvering projectiles for increased lethality is being explored for future weapon systems in various scenarios (e.g., air-to-air, air-to-ground, etc.).[1] Additionally, non-axisymmetric projectiles have been shown to generate large amounts of lift than conventional circular projectiles.[2] However, high speed (Mach > 3.0) maneuvering projectiles has been extremely difficult to attain. Aside from the control system responsible for maneuvering the projectile, the aerodynamics of such configurations at high speeds is still complex due to strong cross-flow influences and flow separation.[3,4,5]

The Flight Vehicles Integration Branch of the Air Force Research Laboratory Munitions Directorate (AFRL/MNAV) has been exploring technologies that specifically addresses issues for such system requirements. Maneuvering projectiles that travel at high speeds have been identified as a requirement for increased lethality against mobile targets.

The work documented herein is part of an international collaborative effort specifically dealing with high-speed weapon integration. Under this collaboration, complementary technical tasks are performed to provide a greater overall understanding of the technology. Comparisons between predictive and experimental data will highlight deficiencies and provide confidence in future system design studies.

Objectives

The overall objectives of the collaborative research effort are:

- To assess the application and relevance of high-speed maneuvering projectiles

- To develop and validate predictive methodologies for these configurations

This paper will present only the aerodynamic results obtained from predictive methodology, free-flight ballistic range trials, and numerical simulations (based upon the flight conditions of the ballistic range trials). The sole configuration studied in this paper is a one-half power-law elliptic cross-section projectile.

Approach

A suitable configuration was selected to perform the aerodynamic analysis. The UK H3[2] was chosen as a baseline configuration since this configuration would fall within the capabilities of the aeroprediction methodology. Additionally, the H3 would be easily tested within the ballistics range and be straightforward for CFD modeling. Subscale ballistic range models were designed and tested within the Aeroballistics Research Facility (ARF) to velocities in excess of Mach 4. A concurrent CFD effort to model the projectile at the conditions of the ballistic range tests was also performed. The data was then compared and regions of agreement and disagreement were highlighted. The result of this study provides confidence in applying the CFD techniques to more advanced configurations.

Model Geometry

The "H3" configuration studied in this effort is depicted in Figure 1. The H3 is a one-half power-law projectile with a 0.6 aspect elliptic cross-section. The cross-sectional variation of the body that is given by the one-half power law is

$$r = kx^{0.5} \qquad (1)$$

where k is a constant for constant θ and the *x-axis* origin is at the nose of the projectile. The H3 length is given as 540 mm and the major base diameter is 60 mm[2]. Note that the length, major base diameter, and elliptic ratio (given as 0.6) are all that is required to define this shape.
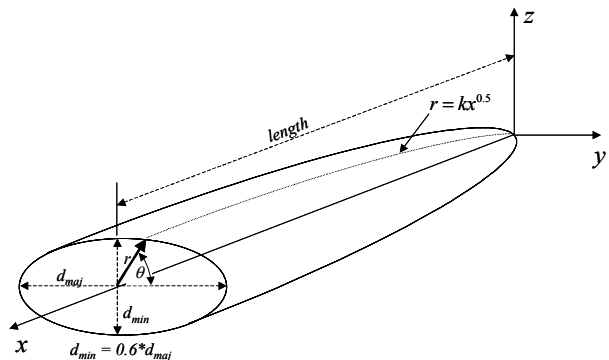

Figure 1. H3 model geometry

Aerodynamic Predictions

Engineering level prediction capability for non-circular cross-section bodies is extremely limited. One of the only known codes for a variety of such configurations is the 1998 version of the US Naval Surface Weapons Center Aeroprediction Code (AP98)[6,7]. Predictions of the H3 configuration were performed[8] and will be presented in the results section of this paper.

Free-Flight Testing

Facility

The tests were conducted in the US Air Force Aeroballistic Research Facility (ARF)[9]. This facility is operated and maintained by the Air Force Research Laboratory Munitions Directorate, Eglin AFB, FL. The ARF is an enclosed, instrumented, concrete structure used to examine the exterior ballistics of various free-flight projectiles. The 207-meter instrumented length of the range has a 16 m^2 square cross section for the first 69 meters and a 25 m^2 square cross section for the remaining length. The range has 131 locations available as instrumented stations of which 50 are currently used to house fully instrumented orthogonal shadowgraph stations. Besides the shadowgraph stations the facility contains one laser-lighted photographic station located in the uprange end of the instrumented section. The range is an atmospheric test facility where the temperature and the relative humidity are controlled to 20 ±1 °C and less than 55% respectively. A chronograph system provides the

times for the projectile at each station. These times together with the spatial position and orientation obtained from the orthogonal photographs provide the basic trajectory data from which the aerodynamic coefficients are extracted.

Model Design

Free-flight testing requires a statically stable model to determine the projectile's aerodynamic coefficients and stability derivatives.[10] A homogeneous H3 projectile would have its center of gravity at approximately 67% of the body length[2]. It was determined through initial predictions[2,8] that the center of pressure is at roughly 50-56% body length. It was then necessary to design a ballistic range model whose CG was ahead of the 50% body length position. Since there was some uncertainty about the exact location of the center of pressure for this configuration, a conservative desired location for the CG was selected at 47% body length.

Since the H3 configuration has more volume in the rear of the projectile, it was necessary to design a model with a heavy nose section and a lighter afterbody. The conventional means to adjust the center of gravity for a ballistic range model is to use a heavier material for the nose than for the base and this was done in these test models.

In order to get the center of gravity for the H3 configuration to 47%, a tungsten nose with an aluminum afterbody was required. Additionally, a hole was placed in the rear afterbody to further lighten the afterbody. The ballistic range model is depicted in Figure 2. Here, the ballistic range model is a 25% scale version of the H3. Additionally, a sabot was required to house the model in the launch
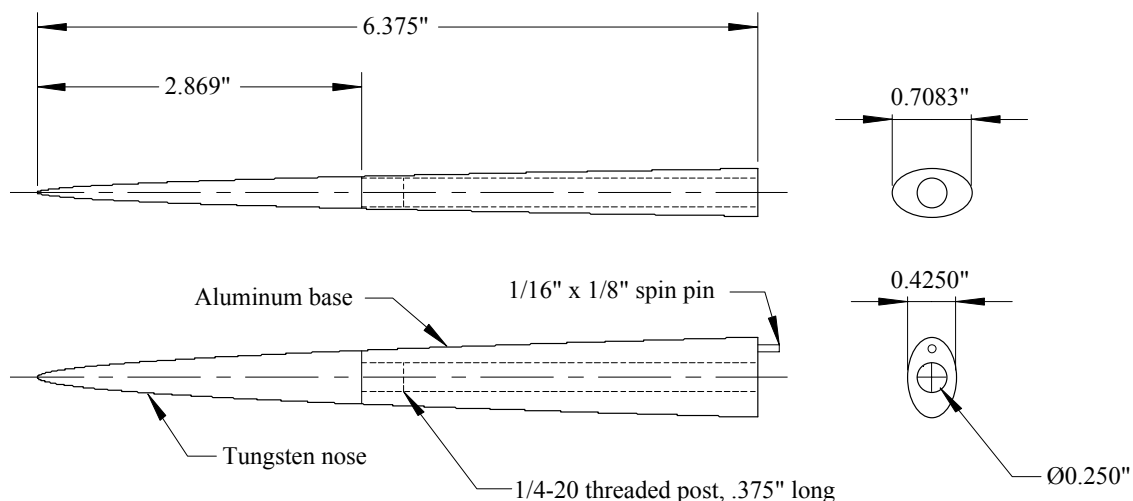

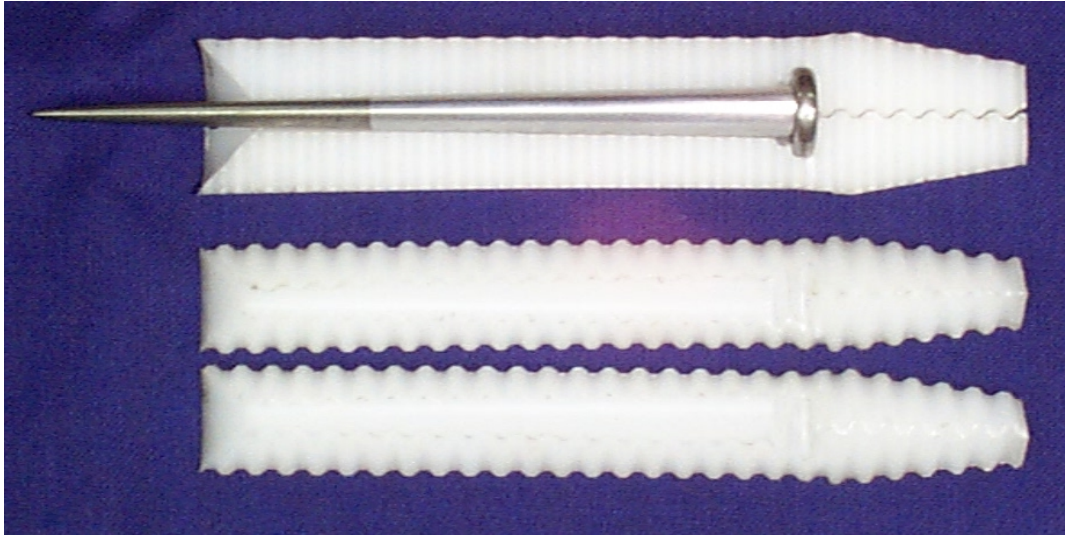
Figure 2. Free-flight ballistic range model

3

Figure 3. Free-flight model sabot

tube. The sabot is shown in Figure 3. The model's physical properties are given in Table 1.

Table 1. Model physical properties

Reference Diameter (d_{maj}), mm	18.00
Reference Area ($A=\pi*d_{maj}*d_{min}$), mm^2	152.68
Length (l), mm	162.0
Mass, g	70.6
I_x, g*cm2	9.34
I_y, g*cm2	1170.
X_{CG}, mm from nose	75.5

Test Conditions

All test firings conducted at the ARF were done at atmospheric pressure. As previously mentioned, the temperature and humidity within the ARF is controlled to about 21°C and 50%, respectively. The launch velocities ranged from Mach 3.0 to just below 5.0. Attempts to increase the launch velocity resulted in damage to the model. This was due to the launch acceleration causing "set-back" loads from the tungsten nose that buckled the aluminum afterbody.

Aerodynamic Parameter Identification

From each set of free flight motion data the aerodynamic force and moment coefficients have been extracted. The essential steps of the data reduction are:
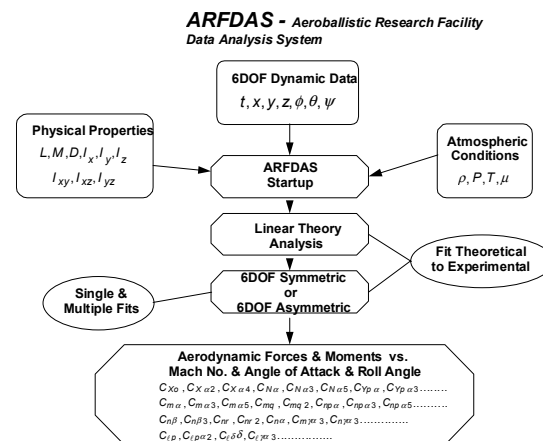

Figure 4. ARFDAS parameter identification process

1) assemble the physical properties and atmospheric conditions,

2) film reading to determine the spatial position and orientation of the model,

3) mathematically modeling the test configuration's theoretical equation of motion, and

4) matching these theoretical equations to the experimental data in order to determine the aerodynamic parameters of the model.

The complete process is described in Reference 11. The Comprehensive Automated Data Reduction and Analysis System (CADRA)[12] is used to read the film and calculate the trajectory. The trajectory matching process is accomplished using the Aeroballistic Research Facility Data Analysis System (ARFDAS)[11,13] and is depicted graphically in Figure 4.

ARFDAS incorporates a standard linear theory analysis[11,13,14] and a six-degree-of-freedom (6DOF) numerical integration technique[15]. The 6DOF integration routine incorporates the Maximum Likelihood Method (MLM) to match the theoretical trajectory to the experimentally measured trajectory.[16] The MLM is an iterative procedure that adjusts the aerodynamic coefficients to maximize a likelihood function. The use of this likelihood function eliminates the inherent assumption in least-squares theory that the magnitude of the measurement noise must be consistent between dynamic parameters (irrespective of units). In general, the aerodynamics can be nonlinear functions of the angle of attack, Mach number, and aerodynamic roll angle.

Each model fired in the ARF was initially analyzed separately, then combined in appropriate groups for simultaneous analysis using the multiple fit capability. This provides a common set of aerodynamics that match each of the separately measured position-attitude-time profiles. The multiple fit approach provides a more complete spectrum of angular and translational motion than would be available from any one trajectory considered separately. This increases the probability that the determined coefficients define the model's aerodynamics over the entire range of test conditions.

Numerical Analysis

Cobalt$_{60}$

Flow fields for the H3 configuration were computed using the June 2000 version of the Cobalt$_{60}$ code that had been developed by the Computational Sciences Branch at the U. S. Air Force Research Laboratory[17]. Cobalt$_{60}$ is an implicit, parallel code that can be used to solve the Navier-Stokes or Euler Equations. Reynolds-Averaged turbulence models available in this version were: Spalart-Allmaras[18], Menter's Baseline[19], Menter's Shear Stress Transport[19], and Wilcox's 1998 k-ω[20] models. Forsythe et al[21] tested these models on numerous benchmark cases, including a Mach 2.5 axisymmetric base flow. Menter's Baseline Model with compressibility correction was used for all the current calculations based on its performance on the base flow test case.

The unstructured grids that were used for the present study were generated using VGRIDns[22]. In order to minimize the computational resources required, the grid generation strategy took advantage of flow-field symmetry. For the zero degree case, only one quarter of the geometry was gridded. For the angle of attack cases, the grid was mirrored using the blacksmith utility[23] to provide a grid that modeled half of the geometry, as shown in Figure 5. The same process was applied for the beta cases. The quarter geometry grid contained 1.65 million cells. The half geometry grids contained double that amount. Prisms were used in the boundary layer, with an average first y$^+$ of 0.8 and a geometric stretching growth rate of 1.25. A close up of the base region is shown in Figure 6.
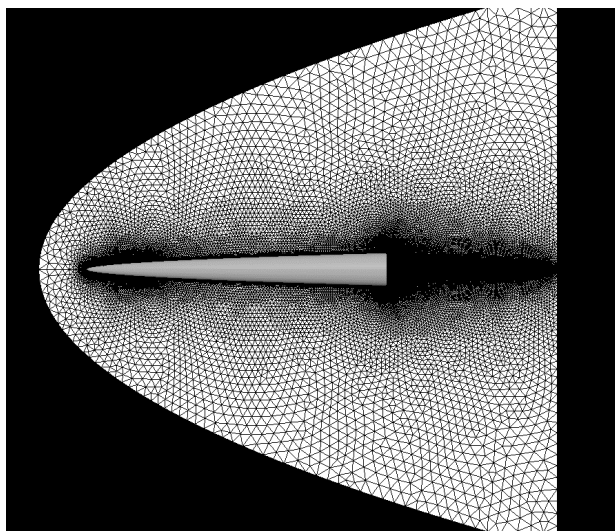

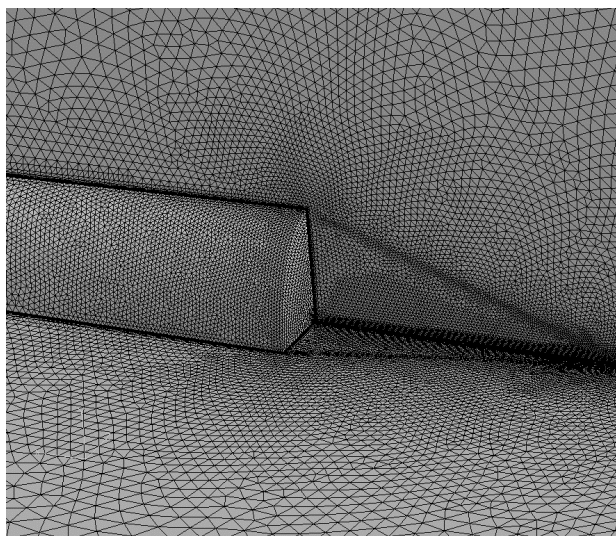Figure 5. Computational domain for the alpha cases

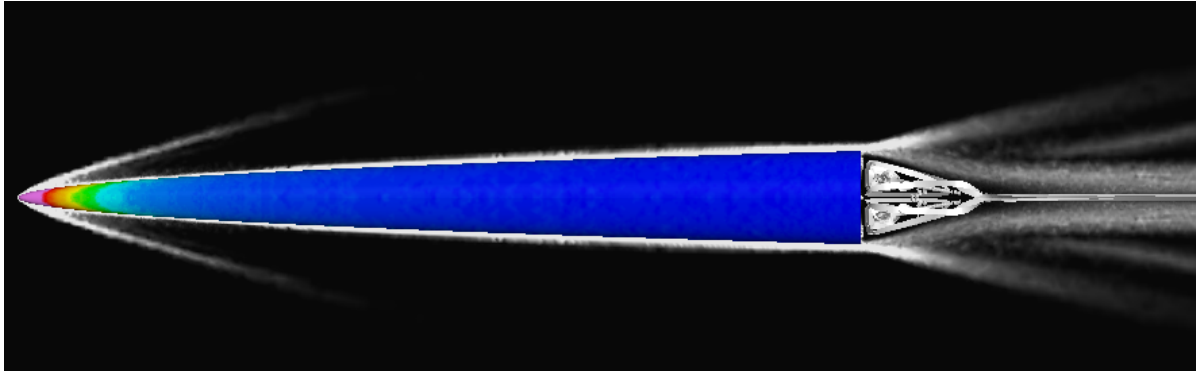Figure 6. Grid close-up view of the base region for the zero degree cases

Figure 7. CFD results for zero alpha - surface colored by pressure, schlieren on the symmetry plane, and streamlines in the base region

The far-field boundaries were located far enough from the surface of the model so that the entire bow-shock wave would be captured (~8.5 reference diameters). The upstream boundary was located approximately 1.4 reference diameters upstream of the nose. The downstream boundary was located far enough downstream from the base (~5.4 reference diameters) to recover to supersonic flow thereby preventing any reflections at the downstream boundary from affecting the solution upstream.

The inflow boundary conditions for the CFD simulations were taken to be representative of the ballistic range tests. A candidate flight condition was chosen at Mach 4.2 and comparable temperature and pressure values consistent with the ballistic range tests were specified.

To calculate values of force and moment derivatives versus alpha and beta, solutions were generated at 0°, 1° alpha and 1° beta. The derivatives were then calculated by comparing the forces and moments at 0° and 1°. By symmetry, all forces and moments except the axial force were zero for 0°.

Axial and normal forces, number of supersonic cells, and average first y^+ values were monitored during the runs to check for convergence. The run was considered converged when these values changed by less than 1% over 500 iterations in a row. This required approximately 4000 iterations. A grid refinement study was not conducted. However sensitivity to grid resolution was explored for the forebody region only previously[24]. A coarser grid than the current one was seen to give grid independent solutions for the pressures at two axial locations. This is certainly not proof of a grid converged solution for the current study, especially in the base region.

Results & Discussions

Aerodynamic Data

For all coefficients and derivatives, the reference length is the major ellipse diameter (d_{maj}) of the base and the reference area is the cross section area of the model base ($A = \pi * d_{maj} * d_{min}$). The moment reference point is about the center of gravity (46.6% from the nose). The complete set of aerodynamic data from the experiments and predictions are presented in Table 2. For the Cobalt$_{60}$ data, the forces and moments were a result of surface integration of the pressure.

The zero yaw axial force coefficient (C_{Xo}) versus Mach number is shown in Figure 8. The shaded symbols are the result of matching multiple flight trajectories to a common set of aerodynamics. Figure 8 shows good agreement between the experimental data and the predictions. The base drag is the dominant drag for a slender projectile such as the H3, so predicting the base pressure is crucial to accurately predicting the drag. For the Mach 2.5 base flow previously examined[21], turbulence models without compressibility corrections were seen to under-predict the base pressure by 40-90%. Menter's Baseline model with compressibility corrections (the model used in the current study) predicted the base pressure to within 12%. The agreement in the current research, therefore, is probably in large part due to the proper choice of turbulence models.

Figure 9 shows the normal force coefficient derivative in the pitch plane ($C_{Z\alpha}$) versus Mach number and Figure 10 shows the yaw plane normal force coefficient derivative ($C_{Y\beta}$) versus Mach number. There is immediately seen a fair amount of scatter in the experimentally-determined values for normal/yaw force derivative. This coefficient is

sometimes difficult to measure accurately from free-flight data if there is not sufficient heaving motion of the projectile[10], which was true in this case. Better agreement is seen with the multiple-fit data. The aeroprediction data (AP98) and CFD data agree very well in the Mach number range shown.

Figure 11 contains the pitching moment coefficient derivative in the pitch plane ($C_{m\alpha}$) as a function of Mach number. Similarly, the yaw plane moment coefficient derivative ($C_{n\beta}$) versus Mach number is shown in Figure 12. There is better consistency in this data vice the force data. Again, this is in general the situation where the angular data is measured well within the free-flight range.

It is seen from the moment data that the H3 configuration is marginally stable and that there is little variation with Mach number. In spite of this marginal stability, there was very little angular motion observed in the experimental data. As seen from the total angle of attack data ($\overline{\alpha}^2$) in Table 2, the angle of attack was only a few degrees at most (with the exception of shot 54). Predictions of the moment data agree very well with the observed data but predict slightly more moment stability in both the pitch and yaw planes.

Figure 13 presents the center of pressure variation with Mach number for this configuration as observed from the data. The center of pressure location for the data of Figure 13 were found via equation (1)[10] which is given as:

$$\frac{X_{c.p.}}{l} = \frac{X_{CG}}{l} - \frac{C_{m\alpha}}{C_{Z\alpha}} \frac{d_{maj}}{l}. \quad (2)$$

Here it is seen that the experimental data has a center of pressure slightly ahead of the predicted values. As can be seen here, the test configuration was just slightly stable. The computational location for the center of pressure is slightly aft of both the free-flight data and the AP98 data.

Pitch damping (C_{mq}) and yaw damping ($C_{n\beta}$) were not adequately determined from the free-flight data due to the small amplitude changes during each flight in the ARF. Trim asymmetries and roll induced side moments resulted in a very complex motion spectrum. A representative value for pitch damping is believed to be about –50.

Figure 14 shows a direct shadowgraph of the H3 projectile obtained in the ARF. This shadowgraph is from shot 67 (Mach 3.32) and shows the shock structure and wake region in nice detail.

Table 2. Aerodynamic Results

	air density (kg/m³)	Speed of sound (m/s)	Mach number	C_{Xo}	$C_{Z\alpha}$	$C_{Y\beta}$	$C_{m\alpha}$	$C_{n\beta}$	X_{cp}/l	$\overline{\alpha}^2$	shot number
Aeroprediction Code (AP98)											
	1.2256	340.27	1.30	0.307	3.566	1.274	-1.291	-0.793	0.506		
	1.2256	340.27	2.00	0.222	3.624	1.294	-1.094	-0.706	0.500		
	1.2256	340.27	3.00	0.158	3.708	1.317	-1.091	-0.697	0.499		
	1.2256	340.27	4.00	0.120	3.744	1.330	-1.156	-0.735	0.500		
	1.2256	340.27	4.28	0.111	3.749	1.332	-1.175	-0.745	0.501		
	1.2256	340.27	5.00	0.092	3.756	1.334	-1.218	-0.774	0.502		
	1.2256	340.27	6.00	0.076	3.387	1.235	-1.174	-0.984	0.505		
	1.2256	340.27	7.00	0.065	3.385	1.233	-1.163	-0.919	0.504		
Free-Flight Range (ARF)											
single fits	1.206	343.7	3.00	0.200	4.170	1.640	-0.953	-0.349	0.474	0.6	66
	1.209	343.0	3.32	0.156	3.720	1.210	-1.061	-0.542	0.476	2.7	67
	1.205	344.1	3.65	0.151	3.200	2.310	-0.992	-0.782	0.476	2.2	65
	1.196	344.2	3.98	0.130	3.490	2.120	-0.899	-0.651	0.475	7.8	56
	1.207	344.3	4.14	0.112	4.870	1.130	-0.914	-0.418	0.472	3.0	63
	1.201	344.6	4.18	0.133	3.560	1.610	-1.356	-0.635	0.479	3.1	64
	1.209	343.7	4.36	0.119	2.430	1.490	-1.526	-0.511	0.487	0.3	62
	1.209	343.6	4.50	0.109	3.070	1.850	-0.992	-0.767	0.477	2.2	61
	1.196	344.2	4.92	0.104	3.750	1.980	-1.580	-0.682	0.480	11.2	54
multiple fits			3.16	0.178	4.270	1.190	-1.286	-0.434	0.476	1.6	66. 67
			3.82	0.149	3.320	2.220	-0.821	-0.674	0.474	5.0	65, 56
			4.27	0.126	2.990	1.460	-1.557	-0.503	0.483	1.8	62, 64
			4.71	0.106	3.570	2.110	-1.061	-0.449	0.476	6.9	61, 54
Cobalt 60											
	1.2256	343.86	4.20	0.107	3.510	1.520	-1.362*	-0.569*	0.522		

* based upon solutions at 0 & 1 degrees α
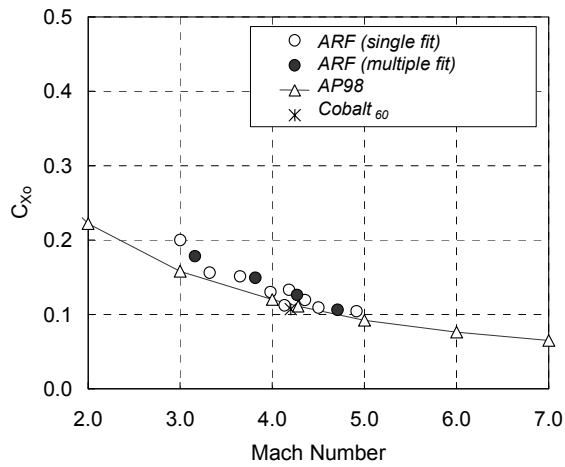
7

Figure 8. Zero-yaw axial force coefficient vs. Mach number
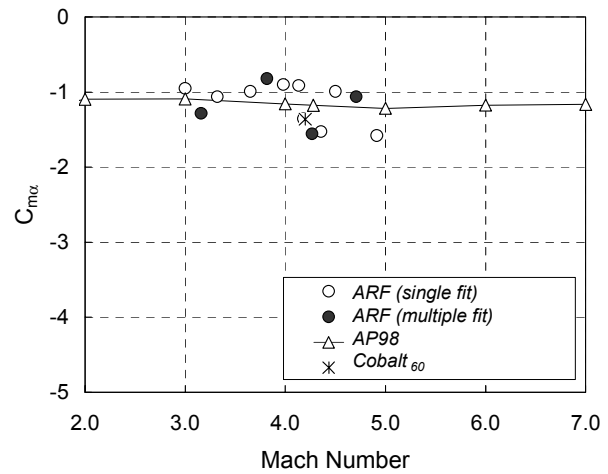

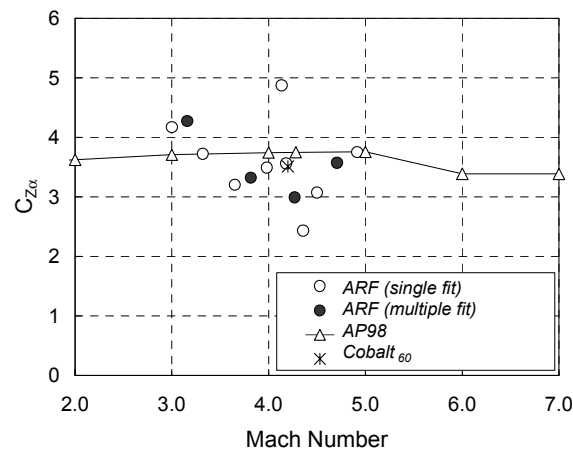Figure 11. Pitch plane moment coefficient derivative vs. Mach number

Figure 9. Pitch plane normal force coefficient derivative vs. Mach number
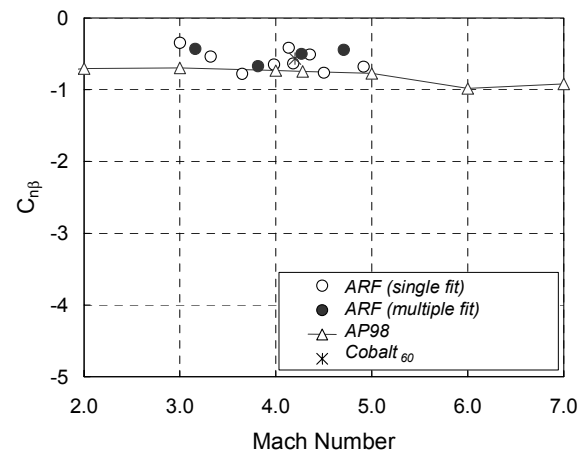

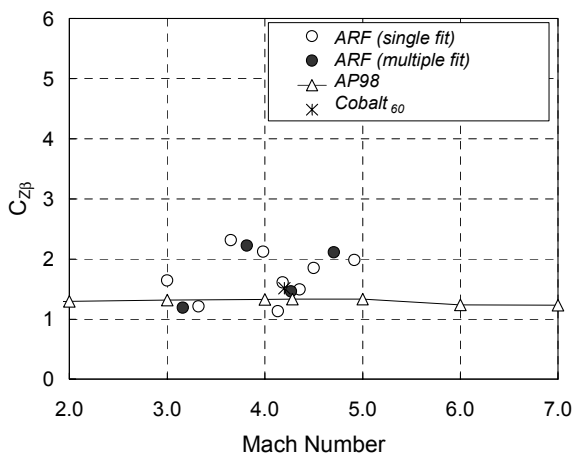Figure 12. Yaw plane moment coefficient derivative vs. Mach number

Figure 10. Yaw plane normal force coefficient derivative vs. Mach number
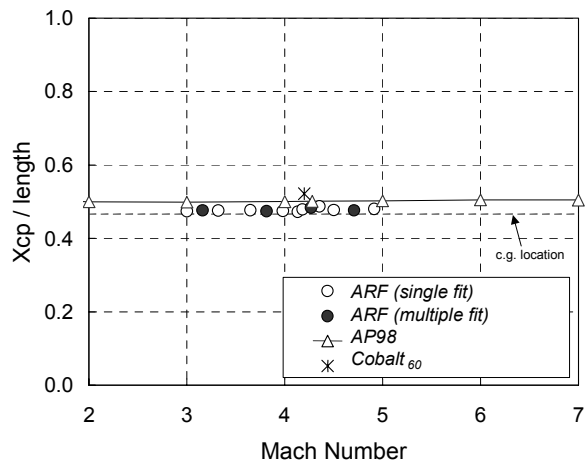

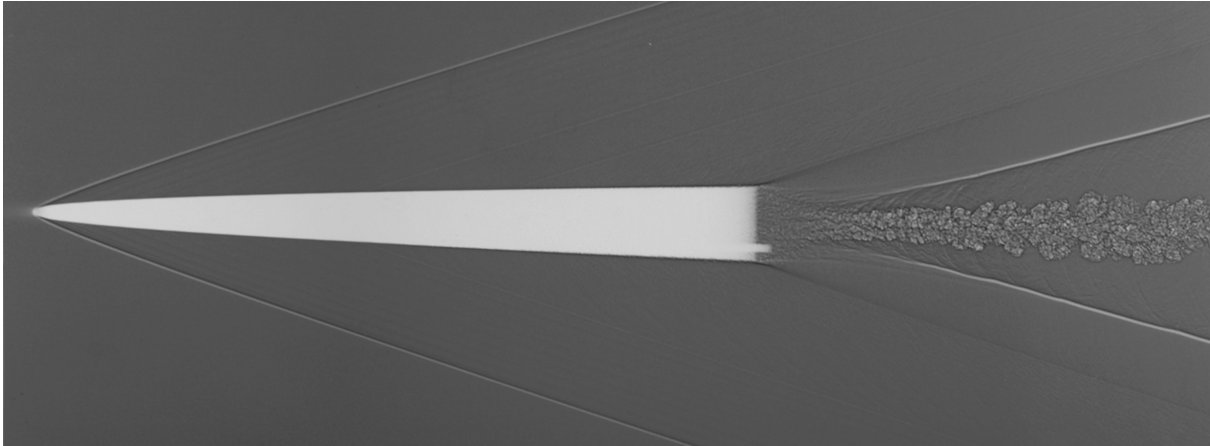Figure 13. Center of pressure variation vs. Mach number

8

Figure 14. Shadowgraph of H3 projectile traveling at Mach 3.32 (shot 67)

Conclusions

Free-flight experiments of a power-law elliptic cross-section projectile have been conducted and analyzed from Mach numbers of 3.0 through 5.0. Aerodynamic stability derivatives and coefficients have been determined from this data. Computational fluid dynamic simulations were run at the Mach 4.2 free-flight conditions and have been compared to the experimental data. The experimental and CFD data were compared with results from an engineering level aeroprediction code (AP98).

Overall, the agreement between the integrated surface pressure coefficients of the numerical method (Cobalt$_{60}$) and engineering method (AP98) with the measurements obtained in the free-flight range is good. This builds confidence in these methods as useful predictive tools for this and similar configurations for preliminary design. To truly validate these tools for an in-depth detailed design study, a grid refinement study would need to be accomplished for the CFD. Additionally, higher amplitude motion would need to be induced in the free-flight projectiles to provide experimental data at higher angles of attack. This will allow better determination of the aerodynamic coefficients and stability derivatives. This will reduce the scatter seen in free-flight results and allow the nonlinear behavior of the coefficients to be determined.

AP98, an empirical based method, was highly efficient, taking only minutes to setup and run a case. AP98 was able to predict the aerodynamics of the H3 reasonably well. Cobalt$_{60}$ complements AP98 since it is able to handle complex geometries through the use of unstructured grids. Solutions take longer, however, with about one day to create the grid, and one day per solution. The advantage of using CFD methods is to predict the entire flowfield, which includes complex phenomena such as separated flow and shock/vortex interaction.

As encouraging as these results are, there was a discrepancy between the prediction methods and free-flight results for the center of pressure, which is the most crucial parameter to predict. A maneuvering projectile would want its center of gravity forward of the center of pressure for stability, but not so far forward as to reduce maneuverability. Grid refinement in the CFD may have reduced this discrepancy.

References

1 Champigny, P and Lacau, RG, "Lateral Control Jets for Tactical Misiles," Paper Number 3 in AGARD Report 804, Special Course, June 1994

2 Edwards, JA and Roper, JJ, "A Computational Assessment of Static and Dynamic Coefficients for the H3 Hypervelocity Projectile," AIAA Paper 97-0640, Jan. 1997

3 Pagan, D, Molton, P, and Delery, J, "Basic Experiment on a Supersonic Vortex Flow Around a Missile Body," Journal of Spacecraft and Rockets, Vol. 29, No. 3, May 1992, pp. 373-378

4 Grasso, F, and Iaccarino, G, "Influence of Crossflow and Turbulence on Vortex Flow Around a Supersonic Missile," Journal of Spacecraft and Rockets, Vol. 35, No. 1, Jan.-Feb. 1998, pp. 37-45

5 Shereda, RE, Amidon, PF, and Dahlem, VI, "Wind-Tunnel Tests of Elliptic Missile Body

Configurations at Mach Numbers 0.4 to 5.0," AFWAL-TR-87-3086, Dec. 1987

6 Moore, FG, McInville, RM, and Hymer, TC, "Review and Extension of Computational Methods for Noncircular Cross-Sectional Weapons," Journal of Spacecraft and Rockets, Vol. 35, No. 5, 1998, pp. 585-597

7 Moore, FG, McInville, RM, and Hymer, TC, "Application of the 1998 Version of the Aeroprediction Code," Journal of Spacecraft and Rockets, Vol. 36, No. 5, 1998, pp. 633-645

8 Moore, FG, private communication

9 Kittlye, RL, Packard, JD, Winchenbach, GL, "Description and Capabilities of the Aeroballistic Research Facility," AFATL-TR-87-08, May 1987

10 Winchenbach, GL, "Aerodynamic Testing In A Free-Flight Spark Range," WL-TR-1997-7006, April 1997

11 Fischer, MA and Hathaway, WH, "ARFDAS Users Manual," AFATL-TR-88-48, November 1988

12 Yates, LA, "A Comprehensive Aerodynamic Data Reduction System For Aeroballistic Ranges," WL-TR-96-7059, Wright Laboratory, Armament Directorate, Eglin AFB, FL, October 1996

13 Hathaway, WH and Whyte, RH, "Aeroballistic Research Facility Free Flight Data Analysis Using The Maximum Likelihood Method," AFATL-TR-79-98, Air Force Armament Laboratory, Eglin AFB, FL, December 1979

14 Murphy, CH, "Free Flight Motion of Symmetric Missiles," BRL Report 1216, Aberdeen Proving Ground, MD, July 1963

15 Murphy, CH "Data Reduction for the Free Flight Spark Ranges," BRL Report 900, Aberdeen Proving Ground, MD, February 1954

[16] MLM ref.

17 Grismer, MJ, Strang, WZ, Tomaro, RF, and Witzeman, FC, "Cobalt, A Parallel, Implicit, Unstructured Euler/Navier-Stokes Solver," Advances in Engineering Software, Vol. 29, No. 3-6, 1998, pp. 365-373

18 Spalart, PR, and Allmaras, SR, "A One-Equation Turbulence Model for Aerodynamic Flows," AIAA 92-0439, January 1992

19 Menter, FR, "Zonal Two Equation k-ω Turbulence Models for Aerodynamic Flows," AIAA 93-2906, 1993

20 Wilcox, DC, Turbulence Modeling for CFD, Second Edition, DCW Industries, Inc., 1998

21 Forsythe, JR, Strang, WZ, Hoffmann, KA, "Validation of Several Reynolds-Averaged Turbulence Models in a 3-D Unstructured Grid Code," AIAA 00-2552, June 2000

22 Pirzadeh, S, "Three-Dimensional Unstructured Viscous Grids by the Advancing-Layers Methods," AIAA Journal, Vol. 34, No. 1, 1996, pp. 257-265

23 http://www.va.afrl.af.mil/vaa/vaac/COBALT/

24 Schuricht, PH, Forsythe, JR, Bertin, JJ, and Abate, GL, "Comparison Between Measurements and Computations for Power-Law Elliptic Section Bodies," AIAA 00-2553, June 2000, Presented at Fluids 2000, Denver, CO